Electronic Structures and Properties of $RE_{12}Ga_4Sb_{23}$ (RE = La−Nd, Sm) and Superconducting $La_{13}Ga_8Sb_{21}$

Allison M. Mills, Laura Deakin, and Arthur Mar*

Department of Chemistry, University of Alberta, Edmonton, Alberta, Canada T6G 2G2

Received December 21, 2000. Revised Manuscript Received February 27, 2001

The bonding in the related structures of $La_{12}Ga_4Sb_{23}$ and $La_{13}Ga_8Sb_{21}$ has been analyzed following a retrotheoretical approach, with the use of extended Hückel calculations. Once the La^{3+} cations have been removed, the $[Ga_4Sb_{23}]^{36-}$ and $[Ga_8Sb_{21}]^{39-}$ metalloid networks can be decomposed into two noninteracting substructures: $[(GaSb_3)_2(Ga_2Sb_{17})]^{36-}$ (in $La_{12}Ga_4Sb_{23}$) and $[(GaSb_3)_2(Ga_6Sb_{15})]^{39-}$ (in $La_{13}Ga_8Sb_{21}$). Trigonal planar $GaSb_3$ units are stacked in a one-dimensional array in $La_{12}Ga_4Sb_{23}$. A pairing distortion results in slight pyramidalization of the $GaSb_3$ units and weak interunit Ga−Ga bonding in the $[GaSb_3]$ substructure of $La_{13}Ga_8Sb_{21}$. The one-dimensional $[GaSb_3]$ stacks are enclosed by networks of Ga-linked square Sb ribbons, $[Ga_2Sb_{17}]$ and $[Ga_6Sb_{15}]$. These networks can be related to a prototypical square sheet of Sb atoms and the oxidation states assigned accordingly. The puckering of the unusual Ga_6 ring that occurs in the $[Ga_6Sb_{15}]$ network of $La_{13}Ga_8Sb_{21}$ is attributed to the stabilization of bands derived from the ring π system by strengthened Ga−Sb bonding to half of the adjacent Sb atoms. When the $La_{12}Ga_4Sb_{23}$ and $La_{13}Ga_8Sb_{21}$ structures are reassembled, the Fermi levels fall in a region of moderate density of states, consistent with metallic behavior. Resistivity measurements for the complete $RE_{12}Ga_4Sb_{23}$ (RE = La−Nd, Sm) series confirm that all are metallic. $La_{13}Ga_8Sb_{21}$ exhibits metallic behavior at high temperatures, but undergoes a metal−superconductor transition at T_c = 2.4 K. Magnetic measurements corroborate this result.

Introduction

Intermetallic compounds M_xA_y or $M_xA_yB_z$ (M = alkali or alkaline-earth metal; A, B = main-group elements) containing a combination of highly electropositive and electronegative components tend to form structures with localized covalent bonding between the electronegative atoms and closed-shell electronic configurations for all atoms.[1] As the electronegativity difference between components decreases, more unusual "nonclassical" metalloid substructures featuring multicenter bonding become prevalent. For instance, many alkali-metal gallide structures display networks of interconnected Ga clusters.[2] The delocalized bonding and nonclassical geometries of these electron-deficient clusters can be explained through the application of Wade's rules.[3] Weak multicenter homoatomic bonding is also observed in the more electron-rich rare-earth antimonides. In these compounds, we find linear chains,[4] square ribbons,[5] and square nets[6] containing, to a first approximation, one-electron Sb−Sb bonds. Electron-counting schemes for these metalloid bonding networks have been detailed in a recent review.[7]

As part of our continuing investigation of the ternary rare-earth main-group antimonide systems, we have recently described the synthesis and characterization of $RE_{12}Ga_4Sb_{23}$ (RE = La−Nd, Sm) and $La_{13}Ga_8Sb_{21}$, the first examples of rare-earth gallium antimonides.[8] The related structures both contain extended Sb−Sb bonding networks and finite Ga−Ga bonded units: nonclassical square ribbons of Sb atoms are linked by either Ga_2 pairs (in $RE_{12}Ga_4Sb_{23}$ (Figure 1)) or by unusual puckered Ga_6 rings (in $La_{13}Ga_8Sb_{21}$ (Figure 2)). Classical trigonal planar $GaSb_3$ units, typically found in $M_xGa_ySb_z$ Zintl compounds,[1] are enclosed within the networks. The structure of the only other rare-earth gallium antimonide reported to date, $REGaSb_2$, also consists of a Zintl component (a $^2_\infty$[GaSb] layer containing strong covalent Ga−Ga and Ga−Sb bonds) and a nonclassical network (a two-dimensional square sheet $^2_\infty$[Sb] containing weak covalent Sb−Sb bonds).[9] Band

* To whom correspondence should be addressed. Telephone: (780) 492-5592. Fax: (780) 492-8231. E-mail: arthur.mar@ualberta.ca.

(1) Eisenmann, B.; Cordier, G. In *Chemistry, Structure, and Bonding of Zintl Phases and Ions*; Kauzlarich, S. M., Ed.; VCH Publishers: New York, 1996; p 61.

(2) For example, see the following. (a) Li_3Ga_{14}: Stöhr, J.; Schäfer, H. *Rev. Chim. Minér.* **1982**, *19*, 122. (b) Na_7Ga_{13}: Frank-Cordier, U.; Cordier, G.; Schäfer, H. *Z. Naturforsch. B: Anorg. Chem., Org. Chem.* **1982**, *37*, 119. (c) KGa_3: Belin, C.; Ling, R. G. *C. R. Séances Acad. Sci., Ser. 2* **1982**, *294*, 1083. (d) $RbGa_7$: Belin, C. *Acta Crystallogr., Sect. B: Struct. Crystallogr. Cryst. Chem.* **1981**, *37*, 2060.

(3) Wade, K. *Inorg. Chem. Radiochem.* **1976**, *18*, 1.

(4) For example, see the following. (a) RE_3MSb_5 (RE = La−Nd, Sm; M = Ti, Zr, Hf, Nb): Bolloré, G.; Ferguson, M. J.; Hushagen, R. W.; Mar, A. *Chem. Mater.* **1995**, *7*, 2229. (b) $Eu_{14}MnSb_{11}$: Rehr, A.; Kauzlarich, S. M. *J. Alloys Compd.* **1994**, *207/208*, 424.

(5) For example, see the following. (a) $RE_6Ge_{5-x}Sb_{11+x}$ (RE = La−Nd, Sm, Gd−Dy): Lam, R.; McDonald, R.; Mar, A. *Inorg. Chem.* **2001**, *40*, 952. (b) RE_6MSb_{15} (RE = La, Ce; M = Mn, Cu, Zn): Sologub, O.; Vybornov, M.; Rogl, P.; Hiebl, K.; Cordier, G.; Woll, P. *J. Solid State Chem.* **1996**, *122*, 266.

(6) For example, see the following. (a) $REIn_{0.8}Sb_2$ (RE = La−Nd): Ferguson, M. J.; Ellenwood, R. E.; Mar, A. *Inorg. Chem.* **1999**, *38*, 4503. (b) $RESn_{0.75}Sb_2$ (RE = La−Nd, Sm): Ferguson, M. J.; Hushagen, R. W.; Mar, A. *Inorg. Chem.* **1996**, *35*, 4505. (c) $RESb_2$ (RE = La−Nd, Sm): Wang, R.; Steinfink, H. *Inorg. Chem.* **1967**, *6*, 1685.

(7) Papoian, G. A.; Hoffmann, R. *Angew. Chem., Int. Ed.* **2000**, *39*, 2408.

(8) Mills, A. M.; Mar, A. *Inorg. Chem.* **2000**, *39*, 4599.

10.1021/cm0014132 CCC: $20.00
Published on Web 04/19/2001

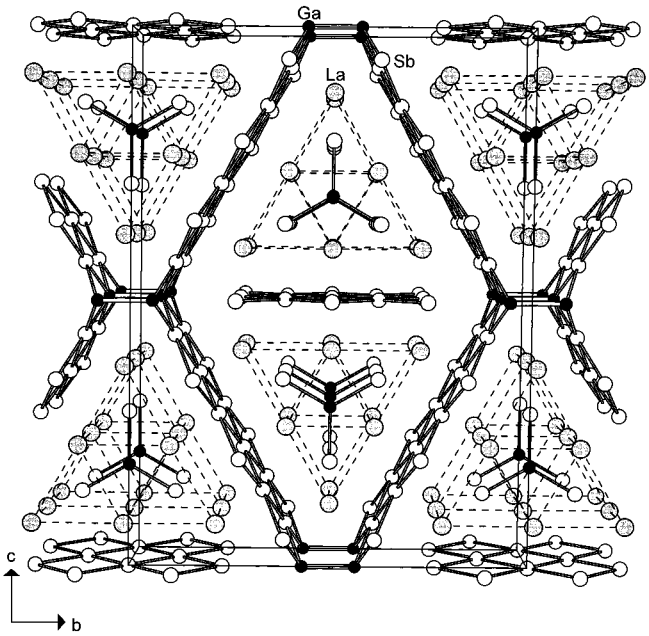

Figure 1. Structure of orthorhombic $La_{12}Ga_4Sb_{23}$ viewed down the *a* axis showing the unit cell outline. The large lightly shaded circles are La atoms, the small solid circles are Ga atoms, and the medium open circles are Sb atoms. The dashed lines merely outline the assemblies of La_6 trigonal prisms.

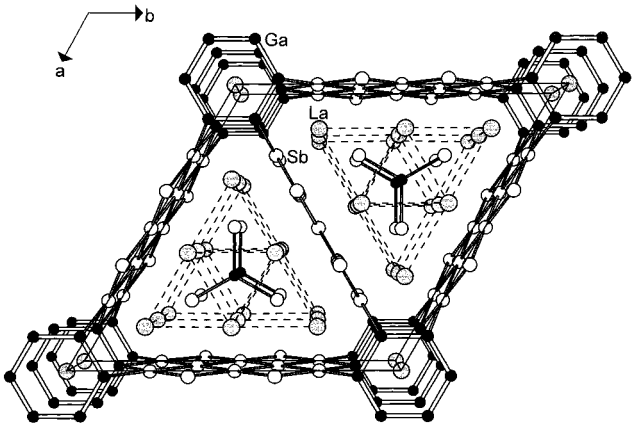

Figure 2. Structure of hexagonal $La_{13}Ga_8Sb_{21}$ viewed down the *c* axis showing the unit cell outline. The large lightly shaded circles are La atoms, the small solid circles are Ga atoms, and the medium open circles are Sb atoms. The dashed lines merely outline the assemblies of La_6 trigonal prisms.

structure calculations for $REGaSb_2$ justified our use of a Zintl analysis to describe the bonding in this compound.

The coexistence of (i) classical moieties that are strongly covalently bonded and finite (Ga_2 pairs, Ga_6 rings, $GaSb_3$ trigonal planes) with (ii) nonclassical networks that are weakly bonded and extended (Sb ribbons), representing the bulk of the structure, implies an interesting electronic situation. Competition develops between localization of electrons in the isolated units and delocalization in the extended networks. Similar structural and electronic characteristics have been identified as prerequisites for the occurrence of superconductivity in several classes of compounds.[10] This paradigm has provided insight into why, for instance, certain rare-earth carbides and carbide halides, with structures consisting of discrete C_2 pairs within an extended metal−metal network of rare-earth atoms, are superconducting.[10c]

We report here the results of band structure calculations for $RE_{12}Ga_4Sb_{23}$ and $La_{13}Ga_8Sb_{21}$ that were performed to clarify the nature of the bonding in these compounds and to examine the applicability of the Zintl concept to these complicated structures. The calculations suggest metallic behavior for both structures, and resistivity measurements of the entire series of compounds confirm this prediction. In addition, one member, $La_{13}Ga_8Sb_{21}$, undergoes a superconducting transition at 2.4 K.

Table 1. Extended Hückel Parameters

atom	orbital	H_{ii} (eV)	ζ_{i1}	c_1	ζ_{i2}	c_2
Ga	4s	−14.58	1.77			
	4p	−6.75	1.55			
Sb	5s	−18.8	2.323			
	5p	−11.7	1.999			
La	6s	−4.89	2.14			
	6p	−4.89	2.08			
	5d	−6.41	3.78	0.77651	1.381	0.45861

Experimental Section

Band Structures. Tight-binding extended Hückel band structure calculations were performed on $La_{12}Ga_4Sb_{23}$ and $La_{13}Ga_8Sb_{21}$ using the EHMACC and YAeHMOP suites of programs.[11−13] (Although the crystal structure determination was on $Pr_{12}Ga_4Sb_{23}$, the La member of the $RE_{12}Ga_4Sb_{23}$ series was chosen for the band structure calculations to allow a better comparison with $La_{13}Ga_8Sb_{21}$. The atomic coordinates used for $La_{12}Ga_4Sb_{23}$ were calculated on the basis of positional parameters from the crystal structure of $Pr_{12}Ga_4Sb_{23}$ and refined cell parameters from the powder pattern of $La_{12}Ga_4Sb_{23}$.[8]) The atomic parameters used are listed in Table 1.[14−17] The full crystal structures of $La_{12}Ga_4Sb_{23}$ and $La_{13}Ga_8Sb_{21}$ were fragmented into lower-dimensional substructures. The band structures for each of these fragment substructures as well as the composite structures were analyzed separately. Mulliken charges and overlap populations were extracted from these separate band structures.

Transport and Magnetic Measurements. $RE_{12}Ga_4Sb_{23}$ (RE = La−Nd, Sm) and $La_{13}Ga_8Sb_{21}$ were prepared as described previously. All transport measurements were made on crystals whose compositions were verified by EDX (energy-dispersive X-ray) analyses on a Hitachi S-2700 scanning electron microscope. Electrical resistivities of single crystals, typically 0.5−1.0-mm-long and 0.05−0.2-mm-wide, were measured with the current parallel to the needle axis (crystallographic *a* axis for $RE_{12}Ga_4Sb_{23}$ or *c* axis for $La_{13}Ga_8Sb_{21}$) by standard four-probe techniques on a Quantum Design PPMS system equipped with an ac-transport controller (Model 7100). A current of 0.1 mA and a frequency of 16 Hz were used. The superconducting transition temperature T_c of $La_{13}Ga_8Sb_{21}$ was

(9) Mills, A. M.; Mar, A. *J. Am. Chem. Soc.* **2001**, *123*, 1151.

(10) For example, see the following. (a) Köckerling, M.; Johrendt, D.; Finckh, E. W. *J. Am. Chem. Soc.* **1998**, *120*, 12297. (b) Fässler, T. F.; Kronseder, C. *Angew. Chem., Int. Ed. Engl.* **1997**, *36*, 2683. (c) Simon, A. *Angew. Chem., Int. Ed. Engl.* **1997**, *36*, 1788.

(11) Whangbo, M.-H.; Hoffmann, R. *J. Am. Chem. Soc.* **1978**, *100*, 6093.

(12) Hoffmann, R. *Solids and Surfaces: A Chemist's View of Bonding in Extended Structures*; VCH Publishers: New York, 1988.

(13) Landrum, G. A. *YAeHMOP: Yet Another extended Hückel Molecular Orbital Package*; http://overlap.chem.cornell.edu:8080/yaehmop.html, 1995.

(14) Ortiz, J. V.; Hoffmann, R. *Inorg. Chem.* **1985**, *24*, 2095.

(15) Hinze, J.; Jaffé, H. H. *J. Phys. Chem.* **1963**, *67*, 1501.

(16) Canadell, E.; Eisenstein, O.; Rubio, J. *Organometallics* **1984**, *3*, 759.

(17) Hughbanks, T.; Hoffmann, R.; Whangbo, M.-H.; Stewart, K. R.; Eisenstein, O.; Canadell, E. *J. Am. Chem. Soc.* **1982**, *104*, 3876.

determined at the point at which the resistivity is 90% of that of the normal state.

For $La_{13}Ga_8Sb_{21}$, magnetic measurements were made on samples totaling ~10−20 mg of individually selected crystals, ground into powders. Magnetic data for $La_{13}Ga_8Sb_{21}$ powders were obtained with a Quantum Design 9T-PPMS dc-magnetometer/ac-susceptometer. ac magnetic susceptibility measurements between 2.0 and 3.2 K were made with a driving amplitude of 1 Oe and a frequency of 1000 Hz. Susceptibility values were corrected for contributions from the gel cap holder diamagnetism and the underlying sample diamagnetism (La, -20×10^{-6}; Ga, -22×10^{-6}; Sb, -15×10^{-6} emu/mol).

Results and Discussion

Retrotheoretical Analysis. Detailed descriptions of the structures of orthorhombic $La_{12}Ga_4Sb_{23}$ (shown in Figure 1 down the *a* axis) and hexagonal $La_{13}Ga_8Sb_{21}$ (shown in Figure 2 down the *c* axis) have been presented previously.[8] The related structures are relatively complex, containing a variety of metalloid substructures. Both structures consist of four-prism columnar assemblies of Ga- or Sb-filled La_6 trigonal prisms residing in channels defined by extended networks of Ga and Sb atoms. By following a "retrotheoretical" analysis, as promoted by Papoian and Hoffmann,[18] we will decompose the three-dimensional structures into more manageable lower dimensional substructures (Figure 3).

We assume, according to the Zintl concept,[19] that the La atoms participate in predominantly ionic bonds by donating their valence electrons to the metalloid substructures. Thus, if we begin by removing La^{3+} cations, we are left with the underlying metalloid frameworks, $[Ga_4Sb_{23}]^{36-}$ (in $La_{12}Ga_4Sb_{23}$) and $[Ga_8Sb_{21}]^{39-}$ (in $La_{13}Ga_8Sb_{21}$). These can each be decomposed further into two noninteracting substructures: the Ga-linked Sb ribbons that outline the channels and the isolated $GaSb_3$ trigonal planes that are contained within them (i.e., $[(Ga_2Sb_{17})(GaSb_3)_2]^{36-}$ and $[(Ga_6Sb_{15})(GaSb_3)_2]^{39-}$). In $La_{12}Ga_4Sb_{23}$, the $[Ga_2Sb_{17}]$ substructure consists of an isolated $[Sb_5]$ ribbon embedded within a $[Ga_2Sb_{12}]$ framework, which in turn can be deconstructed (by breaking Ga−Ga bonds) into strongly kinked $[GaSb_6]$ sheets derived from an idealized square net (Figure 3a). In $La_{13}Ga_8Sb_{21}$, the $[Ga_6Sb_{15}]$ substructure can be deconstructed in two convenient ways: (i) by breaking Ga−Ga bonds to give isolated $[Ga_2Sb_5]$ ribbons or (ii) by breaking Ga−Sb bonds to give Ga_6 rings and $[Sb_5]$ ribbons (Figure 3b).

Determining the distribution of the 36 electrons over the $[Ga_4Sb_{23}]$ substructure or the 39 electrons over the $[Ga_8Sb_{21}]$ substructure is more problematic, and indeed served as an impetus for the band structure calculations. The Sb oxidation states can be assigned by adhering to the generally accepted, and recently summarized, conventions for classical and nonclassical Sb networks.[7] However, the assignment of Ga oxidation states is more ambiguous, given the propensity of Ga to form electron-deficient compounds. Our approach is to assign, on the basis of well-established electron-counting rules, initial charges to the metalloid substructures as we discuss each in turn. For simplicity, we consider only "whole electrons"; as a first approximation,

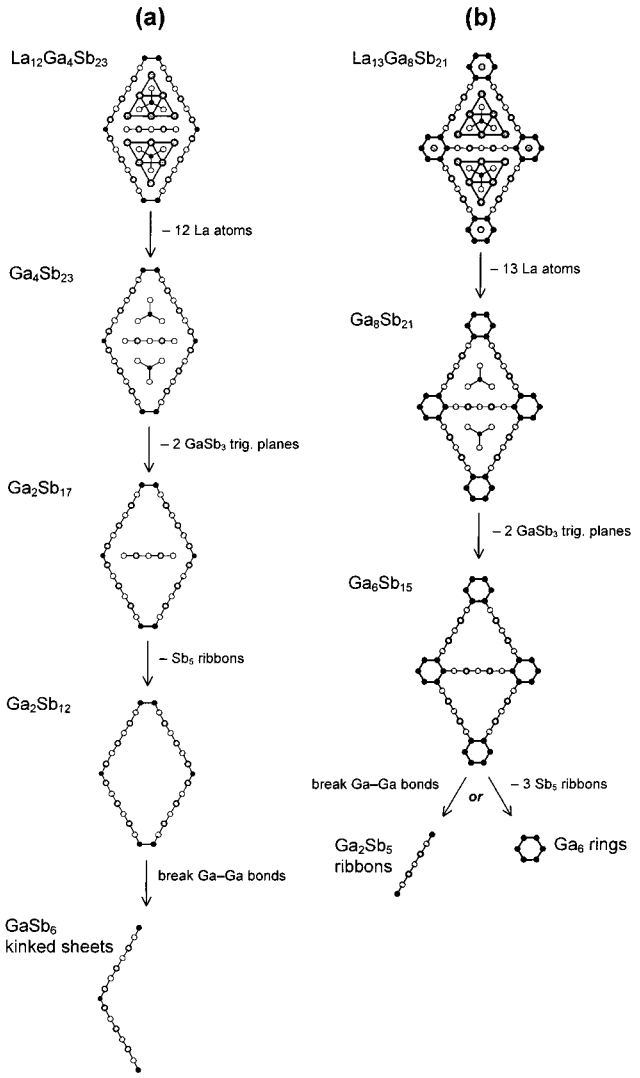

Figure 3. Retrotheoretical analysis of (a) $La_{12}Ga_4Sb_{23}$ and (b) $La_{13}Ga_8Sb_{21}$ in which the complex three-dimensional structures are decomposed into lower dimensional substructures.

σ bonds are described as either one-electron bonds (bond order $^1/_2$) or two-electron bonds (bond order 1). We then re-assemble the substructures into the complete structures and readjust our oxidation state assignments if necessary, following whatever insight we gain from the band structures.

$[GaSb_3]$ Substructures. The simplest structural units found in both $La_{12}Ga_4Sb_{23}$ and $La_{13}Ga_8Sb_{21}$ are the $GaSb_3$ trigonal planes. Similar $GaSb_3$ trigonal planar units are commonly found in classical Zintl compounds, such as the alkali and alkaline-earth metal gallium antimonides.[1] In these compounds, the large electronegativity difference between components supports the use of a Zintl analysis. Thus, for example, in Cs_6GaSb_3, the isolated $GaSb_3$ anions are assigned an overall charge of −6.[20] Within each $GaSb_3^{6-}$ anion, the assignment of oxidation states is straightforward. We first complete the octets of the more electronegative Sb atoms and arrive at an oxidation state of −3 for each Sb atom. The central Ga atom, participating in three

(18) Papoian, G.; Hoffmann, R. *J. Solid State Chem.* **1998**, *139*, 8.
(19) *Chemistry, Structure, and Bonding of Zintl Phases and Ions*; Kauzlarich, S. M., Ed.; VCH Publishers: New York, 1996.
(20) Blase, W.; Cordier, G.; Somer, M. *Z. Kristallogr.* **1992**, *199*, 277.

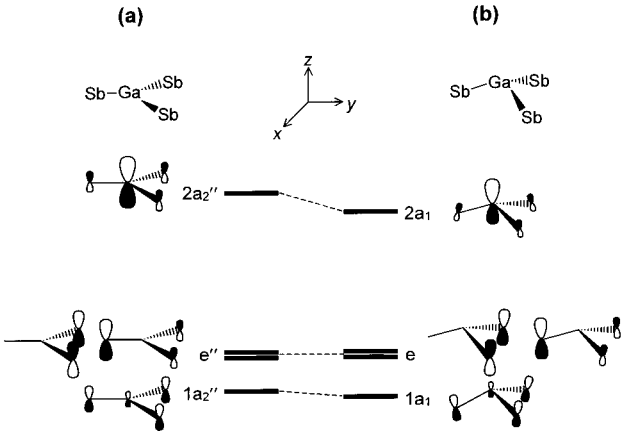

Figure 4. Molecular orbital (MO) schemes for the π systems of (a) planar $GaSb_3$ and (b) pyramidally distorted $GaSb_3$. The main consequence of a slight pyramidalization of the $GaSb_3$ unit is a stabilization of the antibonding π* MO.

Ga−Sb bonds, is assigned an oxidation state of +3 and remains formally electron-deficient.

In all of the alkali and alkaline-earth gallium antimonides, the $GaSb_3^{6-}$ anions are rigorously planar,[1] and the Ga−Sb bond lengths (e.g., 2.608(5)−2.676(5) Å in Cs_6GaSb_3)[20] are somewhat shortened with respect to normal Ga−Sb single bonds (e.g., 2.709(2)−2.752(5) Å in the isolated $GaSb_4^{9-}$ tetrahedra in $Na_3Sr_3GaSb_4$).[21] Partial double bond character has previously been suggested to explain these experimental observations.[22] Molecular orbital calculations performed for a planar $GaSb_3^{6-}$ anion confirm that π bonding does make a significant contribution (Mulliken overlap population (MOP) of 0.08 for Ga($4p_z$)−Sb($5p_z$)) to the strength of the Ga−Sb bonds (MOP of 0.75). Analogous to these classical Zintl anions, the planar geometry and shortened bond lengths (2.647(2)−2.666(2) Å) of the $GaSb_3$ units found in $La_{12}Ga_4Sb_{23}$ lead us to assign an overall charge of −6 to this substructure.

Whereas the $GaSb_3$ units are planar in $La_{12}Ga_4Sb_{23}$, they are pyramidally distorted from the ideal planar geometry in $La_{13}Ga_8Sb_{21}$. The central Ga atoms are shifted slightly (∼0.3 Å) above or below the plane of the Sb atoms (the Ga atoms are disordered over two close sites, each approximately 50% occupied), and the Sb−Ga−Sb angles are 118.81(4)°. This pyramidalization is reminiscent of the well-known trigonal planar to pyramidal distortion of GaX_3 species that accompanies the formation of Lewis acid−base adducts.[23] Our calculations reveal that the buildup of additional electron density at the central Ga atom is responsible for the distortion of the $GaSb_3$ units in $La_{13}Ga_8Sb_{21}$. As shown in Figure 4, the main effect of the slight pyramidalization is the stabilization of the antibonding π orbital ($2a_2''$ in planar and $2a_1$ in pyramidally distorted $GaSb_3$), the result of improved overlap between the s−p hybridized Ga and Sb orbitals. At the electron count proposed above for the $GaSb_3^{6-}$ anion of $La_{12}Ga_4Sb_{23}$, the lowest unoccupied molecular orbital (LUMO) is the antibonding π orbital. Upon addition of any electrons to the system, the distorted geometry becomes energetically favored. Because the $GaSb_3$ units of $La_{13}Ga_8Sb_{21}$ are only slightly distorted from the ideal planar geometry and contain Ga−Sb bond lengths (2.620(2) Å) that are significantly shorter than typical single bonds, we will assume, for simplicity in electron counting, that the reduction of the Ga center occurs through the addition of one electron, that is, $GaSb_3^{7-}$.

Although we have initially considered the $GaSb_3$ trigonal planar units as isolated anions, they are actually stacked along the short axis (∼4 Å) of the structures of both $La_{12}Ga_4Sb_{23}$ and $La_{13}Ga_8Sb_{21}$. We performed band structure calculations on the one-dimensional array of $GaSb_3$ units in $La_{13}Ga_8Sb_{21}$ to examine the possibility that weak Ga−Ga bonding interactions are the driving force for the observed pyramidal distortion. The Ga−Sb antibonding π orbitals (mainly Ga(p_z) in character) of adjacent $GaSb_3$ trigonal planes have the correct symmetry to interact in a σ-type fashion along the stacking axis. If we assemble a one-dimensional stack of planar $GaSb_3^{6-}$ anions (**1**), the Ga−Sb antibonding π LUMO broadens into a band with Ga−Ga σ-antibonding character at the center of the Brillouin zone (Γ) and Ga−Ga σ-bonding character at the edge (Z) (Figure 5a). Adding one electron per $GaSb_3$ unit to the system leads to a half-filled band, making the one-dimensional stack prone to a Peierls distortion.[12]

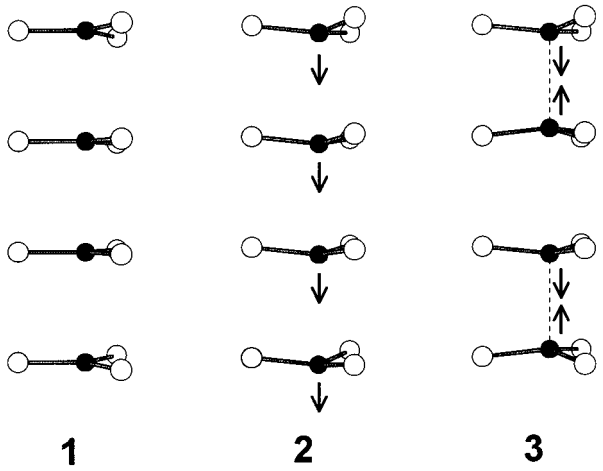

Two local stacking arrangements exist for the disordered $GaSb_3$ units in $La_{13}Ga_8Sb_{21}$: adjacent pyramidal $GaSb_3$ units may be either parallel, with an interunit Ga−Ga distance of 4.338(1) Å that is determined by the *c* parameter, or inverted with respect to one another, such that a shortened Ga−Ga distance of 3.763(1) Å results. We examined both of the limiting one-dimensional arrangements (i.e., all adjacent $GaSb_3$ units parallel—a sliding distortion (**2**); or all adjacent $GaSb_3$ units inverted—a pairing (Peierls) distortion (**3**)). The sliding distortion results in only a slight overall lowering of the energy of the Ga−Sb antibonding band. To prepare for the pairing distortion, the *c* parameter is doubled (and the *c** parameter is halved) so that the bands are "folded back" and the Bloch function midway between Γ and Z in Figure 5a would correspond to a degenerate pair at Z near −5 eV in Figure 5b. The effect of the pairing distortion (**3**) is dramatic: it removes the degeneracy, opening up an energy gap between two

(21) Somer, M.; Carrillo-Cabrera, W.; Nuss, J.; Peters, K.; von Schnering, H. G.; Cordier, G. *Z. Kristallogr.* **1996**, *211*, 479.
(22) Cordier, G.; Ochmann, H. *Z. Naturforsch. B: Chem. Sci.* **1990**, *45*, 277.
(23) Albright, T. A.; Burdett, J. K.; Whangbo, M.-H. *Orbital Interactions in Chemistry*; John Wiley and Sons: New York, 1985.

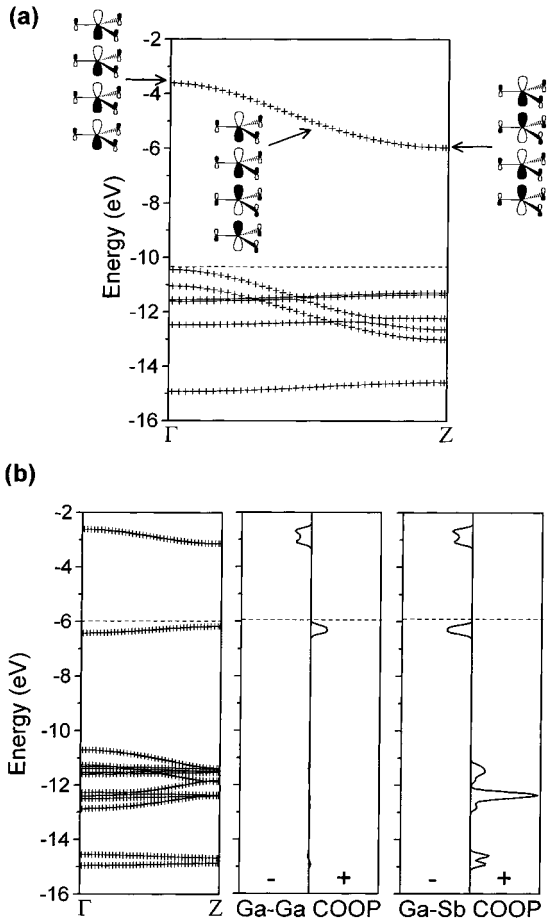

Figure 5. (a) Band structure for a one-dimensional stack of planar $GaSb_3^{6-}$ units (**1**), with the composition of crystal orbitals shown at different wave vectors in the lowest unoccupied band. (b) Band structure for a one-dimensional stack of paired pyramidal $GaSb_3^{7-}$ units (**3**), and the crystal orbital overlap population (COOP) curves for the interunit Ga−Ga and intraunit Ga−Sb interactions. The dashed horizontal lines in (a) and (b) represent the Fermi levels for the $[GaSb_3]^{6-}$ and $[GaSb_3]^{7-}$ substructures at the proposed electron counts.

manifolds in which Ga−Ga bonding states are stabilized and Ga−Ga antibonding states are destabilized, as confirmed by inspection of the Ga−Ga crystal orbital overlap population (COOP) curve (Figure 5b). On the basis of our assignment of a −7 charge per $GaSb_3$ unit, the pairing distortion is clearly preferred energetically. At this electron count, the interunit Ga−Ga bonding is maximized (MOP of 0.41), but the Ga−Sb bond strength is reduced (MOP of 0.66) because more Ga−Sb antibonding levels are populated (Figure 5b). The Mulliken charge determined for the central Ga atom decreases from +0.79 for $[GaSb_3]^{6-}$ to −0.04 upon addition of one electron per $GaSb_3$ unit to the system, while the average Mulliken charge calculated for the Sb atoms remains relatively constant (ca. −2.3).

Although these results support the possibility that individual one-dimensional $[GaSb_3]$ stacks in $La_{13}Ga_8Sb_{21}$ undergo a pairing distortion, there was no evidence for superstructure from the crystal structure determination.[8] This is not surprising, considering that the stacks are far apart from each other (Figure 2). A random distribution of these stacks, while each individually ordered, would still give rise to an overall disorder in the structure.

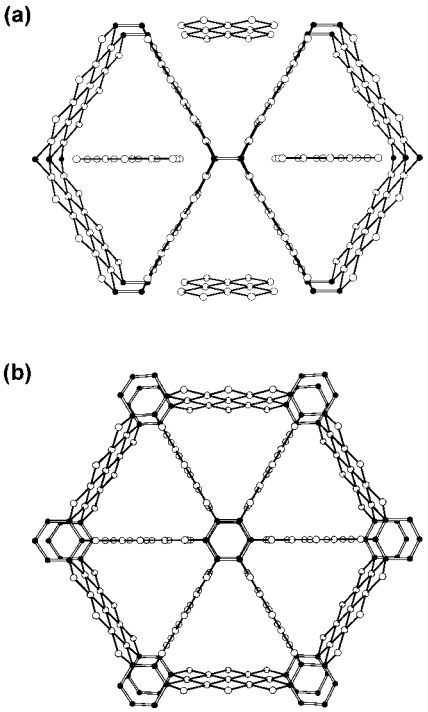

Figure 6. View of the channel-defining (a) $[Ga_2Sb_{17}]$ network in $La_{12}Ga_4Sb_{23}$ and (b) $[Ga_6Sb_{15}]$ network in $La_{13}Ga_8Sb_{21}$. In (a), six-atom-wide Sb ribbons are linked by Ga_2 pairs, resulting in a three-dimensional $[Ga_2Sb_{12}]$ network, while one five-atom-wide ribbon $[Sb_5]$ remains isolated. In (b), five-atom-wide Sb ribbons are linked by Ga_6 rings to complete the three-dimensional substructure.

Sb Ribbons. The most striking recurring theme in the structures of many Sb-rich ternary rare-earth antimonides is the occurrence of Sb networks that contain relatively long Sb−Sb bonds in the 3.0−3.2-Å range,[4−6] longer than a single bond (e.g., 2.81−2.88 Å in KSb)[24] but shorter than the van der Waals contact (∼4.4 Å).[25] While square sheets of Sb atoms in this bonding range are encountered in numerous binary and ternary antimonides,[6] the structures of $La_{12}Ga_4Sb_{23}$ and $La_{13}Ga_8Sb_{21}$ point to a fecundity in bonding patterns that was previously unimaginable, but implied in the structures of α- and β-$ZrSb_2$,[26] and more recently, La_6MnSb_{15}[5b]—ribbons of varying widths can be excised from a square net.

As shown in Figure 6, $La_{12}Ga_4Sb_{23}$ and $La_{13}Ga_8Sb_{21}$ contain complex $[Ga_2Sb_{17}]$ and $[Ga_6Sb_{15}]$ substructures, respectively, that feature nonclassical electron-rich networks of Ga and Sb atoms and which are undeniably beautiful. In both substructures, five- or six-atom-wide square Sb ribbons form the walls of large channels. These can be derived from a prototypical square sheet, for which a well-developed bonding theory exists.[7] According to a hypervalent bonding model, the weak Sb−Sb bonds within the square sheets are described as one-electron bonds, to a first approximation. Implicit in this model are the assumptions that little s−p mixing occurs and that π bonding between Sb atoms is weak. Each Sb atom uses two p orbitals, each accommodating

(24) Busmann, E.; Lohmeyer, S. *Z. Anorg. Allg. Chem.* **1961**, *312*, 53.
(25) Pauling, L. *The Nature of the Chemical Bond, Third Edition*; Cornell University Press: Ithaca, NY, 1960.
(26) Garcia, E.; Corbett, J. D. *J. Solid State Chem.* **1988**, *73*, 452.

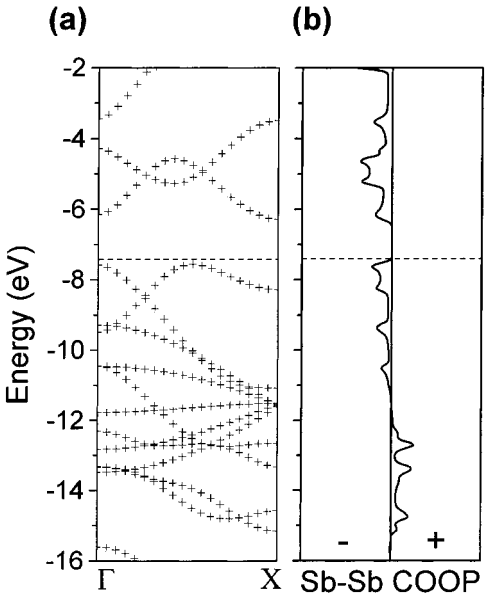

Figure 7. (a) Band structure and (b) Sb−Sb crystal orbital overlap population (COOP) curve for the one-dimensional $[Sb_5]^{7-}$ substructure of $La_{12}Ga_4Sb_{23}$. The dashed horizontal lines in (a) and (b) represent the Fermi level at the proposed electron count.

one electron, to form the in-plane bonds and the remaining p and s orbitals accommodate lone pairs to complete the Sb octets. Correspondingly, each Sb atom of a square sheet, and by extension, an "inner" Sb atom within a ribbon, is assigned an oxidation state of −1. This model will serve as a basis for our description of the bonding in the actual $[Ga_2Sb_{17}]$ and $[Ga_6Sb_{15}]$ substructures.

$[Ga_2Sb_{17}]$ Substructure in $La_{12}Ga_4Sb_{23}$. In $La_{12}Ga_4Sb_{23}$, the channel walls are defined by one five-atom-wide Sb ribbon and two eight-atom-wide sides composed of six-atom-wide Sb ribbons bordered by Ga atoms (Figure 6a). The eight-atom-wide sides are connected by Ga−Ga bonding, but the five-atom-wide Sb ribbon is isolated (the closest contact between this side and the others is ∼4 Å). The anionic $[Ga_2Sb_{17}]$ network can, therefore, be dissected into two noninteracting substructures, the one-dimensional $[Sb_5]$ ribbon and the three-dimensional $[Ga_2Sb_{12}]$ network. These substructures in $La_{12}Ga_4Sb_{23}$ are even more complicated than those found in the closely related La_6MnSb_{15} structure: an $[Sb_3]$ ribbon and an $[Sb_{10}]$ network (referred to as an $[Sb_{20}]$ network in the original paper).[5b] A detailed band structure calculation was performed for La_6MnSb_{15},[18] and we follow a similar approach here.

The $[Sb_5]$ ribbon, containing 3.167(2) Å Sb−Sb bond distances, may be considered as a segment excised from the two-dimensional Sb square sheet described above and the oxidation states of the component Sb atoms assigned accordingly (**4**). The inner Sb atoms are assigned an oxidation state of −1, while the terminal Sb atoms, participating in only two one-electron bonds, require three lone pairs of electrons to complete their octets and are assigned an oxidation state of −2. Thus, we arrive at an overall charge of −7 for the $[Sb_5]$ ribbon. The band structure and Sb−Sb COOP curve calculated for the $[Sb_5]^{7-}$ ribbon are shown in Figure 7. The

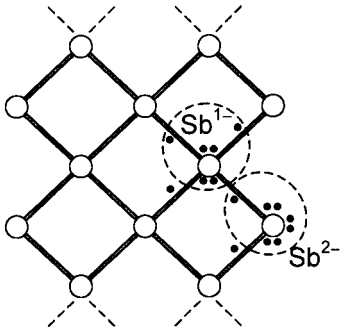

4

calculations confirm our oxidation state assignments: the average Mulliken charges determined for the inner and terminal Sb atoms are −1.00 and −2.00, respectively. At the proposed electron count, some Sb−Sb antibonding states have been filled (Figure 7b), and the overlap population determined for the Sb−Sb bonds is 0.20, within the range observed for the longer Sb−Sb contacts in Sb square sheets,[6a,9] and consistent with bond length correlations.[18]

The $[Ga_2Sb_{12}]$ substructure may be described as a stacking (along the *b*-axis) of strongly kinked $[GaSb_6]$ sheets, each derived from an idealized two-dimensional Sb square sheet (Figures 1, 3a, and 6a). The first step in this transformation is the substitution of Ga for Sb along every seventh diagonal of the sheet. As above, we can assign oxidation states to the atoms of this hypothetical structure: the substituted Ga atoms, with two lone pairs, are assigned as Ga^{1-}, the neighboring Sb atoms as Sb^{2-}, and the remaining Sb atoms as Sb^{1-}. The sheet is then folded along the Ga-substituted diagonal to produce a kinked sheet. In the related La_6MnSb_{15} structure, it was found that the kinking of an $[Sb_{10}]$ sheet, accompanied by s−p hybridization, produces relatively localized lone pairs at the corner Sb atoms.[18] Because lighter elements undergo s−p hybridization more readily than their heavier counterparts,[27] it is quite satisfying to find that kinking in the $[GaSb_6]$ sheet occurs along the Ga-substituted diagonals. As shown in Figure 8a, the localization of the lone pairs on the Ga atoms is reflected by the narrowness of the bands that involve contributions from the Ga(p_y) orbitals, which are perpendicular to the $[GaSb_6]$ sheet (note the Ga(p_y) projection accounting for the large spike near −7 eV in the DOS). When the kinked nets are stacked perpendicular to the *b* direction, the lone pairs on the Ga atoms of adjacent sheets are directed toward each other. Oxidation of the Ga atoms allows intersheet Ga−Ga bonding to occur (**5**); neighboring $[GaSb_6]$ sheets are

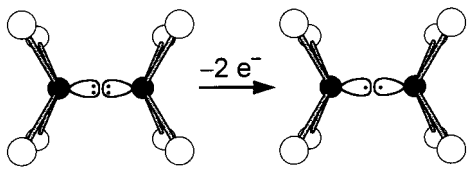

5

thus connected to complete the three-dimensional $[Ga_2$-

(27) Kutzelnigg, W. *Angew. Chem., Int. Ed. Engl.* **1984**, *23*, 272.

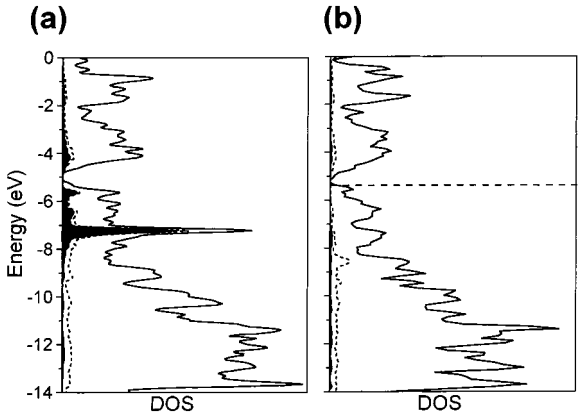

Figure 8. Density of states (DOS) for (a) the two-dimensional kinked $[Ga_2Sb_{12}]$ sheet, and (b) the actual three-dimensional $[Ga_2Sb_{12}]^{16-}$ substructure of $La_{12}Ga_4Sb_{23}$ after Ga−Ga bonds are formed. In (a), the Ga projection is shown by the short dashed line, and the filled area of this curve represents the Ga(p_y) projection; what remains of the DOS is the Sb projection. Initially, the p_y orbitals participate in narrow (localized) bands. After Ga−Ga bond formation, the Ga(p_y) orbitals participate in more dispersive bonding and antibonding bands. The dashed horizontal line in (b) represents the Fermi level for $[Ga_2Sb_{12}]^{16-}$ at the proposed electron count.

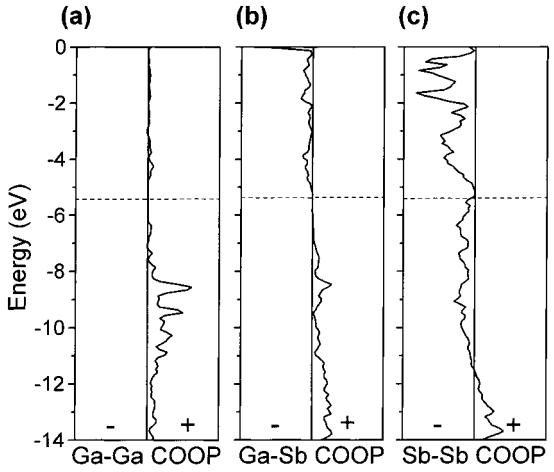

Figure 9. Crystal orbital overlap population (COOP) curves for the (a) Ga−Ga, (b) Ga−Sb, and (c) Sb−Sb interactions in the three-dimensional $[Ga_2Sb_{12}]^{16-}$ substructure of $La_{12}Ga_4Sb_{23}$. The dashed horizontal lines in (a)−(c) represent the Fermi level at the proposed electron count.

Sb_{12}] network. In the DOS curve for the actual [Ga_2Sb_{12}] substructure, the Ga p_y orbitals, now involved in Ga−Ga bonding, are dispersed over a wider energy range (Figure 8b). Although the observed 2.632(2) Å Ga−Ga distance is somewhat longer than the 2.541(3) Å Ga−Ga single bond found in the Zintl compound $Na_2Ga_3Sb_3$,[28] we will approximate it as a single bond. We assign an oxidation state of 0 to the Ga atoms and an overall charge of −16 to the [Ga_2Sb_{12}] substructure. The Mulliken charges determined for the Ga atoms (+0.05), adjacent Sb atoms (−1.66), and inner Sb atoms (−1.18) at this electron count are in good agreement with our proposals. Inspection of the Ga−Ga COOP curve reveals that essentially all of the Ga−Ga bonding states are filled (Figure 9a). The overlap population of 0.77 determined for the Ga−Ga interactions is typical of a single bond. The COOP curves for the Ga−Sb and Sb−Sb interactions within the kinked square sheet are similar, but shifted in energy because of the differing electronegativities of the atoms involved (Figures 9b,c). Fewer Ga−Sb than Sb−Sb nonbonding and antibonding states are filled, and the overlap populations calculated for the 2.956(2) Å Ga−Sb (0.41) and 3.064(2)−3.187(2) Å Sb−Sb (0.14) interactions reflect this. Both overlap populations are reduced with respect to those of full single bonds, supporting our description of these interactions as half-bonds in our simplified model.[9,18]

[Ga_6Sb_{15}] Substructure in $La_{13}Ga_8Sb_{21}$. In the [Ga_6Sb_{15}] substructure of $La_{13}Ga_8Sb_{21}$, three equivalent segments outline the large channels. Five-atom-wide Sb square ribbons are bordered by Ga atoms, forming seven-atom-wide channel walls (Figure 6b). In this case, strong Ga−Ga interactions link all of the walls, and unusual puckered Ga_6 rings are generated at the interface of six wall-sharing channels. The resulting three-dimensional [Ga_6Sb_{15}] network in $La_{13}Ga_8Sb_{21}$ can be analyzed by two approaches. We could proceed as before, considering Ga as a substituent in an otherwise all-Sb network. Here, we would propose that the [Ga_6Sb_{15}] network is assembled by connecting three idealized isolated one-dimensional [Ga_2Sb_5] ribbons per unit cell, with Ga atoms at the terminal positions of each ribbon (Figure 3b). If we assume complete octets for all of the ribbon atoms, we arrive at the following oxidation state assignments: −3 for the terminal Ga atoms, −2 for the adjacent Sb atoms, and −1 for the inner Sb atoms (**6**).

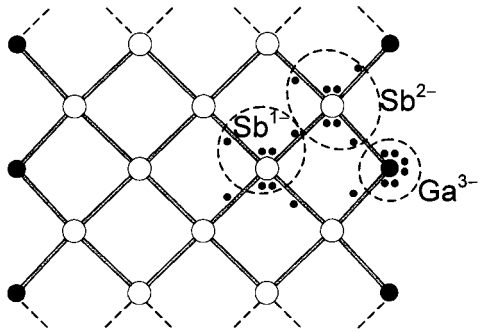

6

According to our model, the terminal Ga atoms, each participating in two one-electron Ga−Sb bonds, have three lone pairs of electrons. When we bring the idealized ribbons together, each Ga atom must be oxidized by two electrons to form two Ga−Ga single bonds involving σ overlap of s−p hybrid orbitals, analogous to the process described earlier in **5**. One lone pair of electrons remains at each Ga^{1-} atom of the resultant planar six-membered rings. Even this admittedly crude electron counting scheme leads to the implication that, for π bonding to play a role in the Ga−Ga bonding within the rings, further oxidation of the Ga centers must take place.

Because the electronic structure of planar six-membered rings is well-known, we can shift our focus, in a second approach to understanding the [Ga_6Sb_{15}] substructure, to the Ga_6 rings and consider what happens when they interact with [Sb_5] ribbons. The molecular

(28) Cordier, G.; Ochmann, H.; Schäfer, H. *Mater. Res. Bull.* **1986**, *21*, 331.

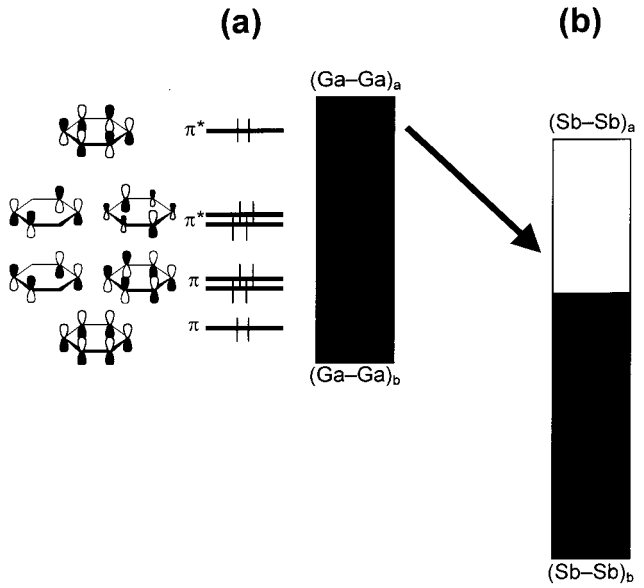

Figure 10. (a) When stacked into a one-dimensional array, the π MOs of a planar Ga_6 ring broaden into a block of states with Ga−Ga bonding character at low energy and Ga−Ga antibonding character at high energy. (b) Electrons from the top of the Ga−Ga π block are transferred to empty Sb−Sb antibonding levels available in the Sb block of an $[Sb_5]$ ribbon.

orbitals involving π overlap in an isolated planar Ga_6 ring are completely filled if we begin with the electron counting scheme above and assume that the lone pair of each Ga^{1-} atom resides in a p_z orbital (Figure 10a). When the Ga_6 rings are stacked in a one-dimensional array, these π-type molecular orbitals transform to a manifold of bands with little dispersion (because there is little interaction between the rings) and which are also completely filled. Now the $[Sb_5]^{7-}$ ribbons, whose band structure was examined earlier, are allowed to interact with the stack of Ga_6 rings. There are still some Sb−Sb antibonding levels that are unoccupied and are lower in energy than the top of the Ga π block, mostly Ga−Ga π antibonding in character (Figure 10b). We thus expect a transfer of electrons to occur in which Ga atoms are further oxidized and Sb atoms are further reduced, allowing Ga−Ga bonding to strengthen at the expense of a slight weakening of the Sb−Sb bonds within the $[Sb_5]$ ribbons.

In the actual crystal structure, the ring Ga atoms are disordered over two sites. The Ga_6 rings are assumed to be puckered into a chair conformation (Ga−Ga−Ga 115.9(3)°) to allow reasonable intraring Ga−Ga distances of 2.422(5) Å. The puckering of these Ga_6 rings is reminiscent of similar distortions seen with stacked 6^3 ("honeycomb") nets such as in the $CaIn_2$-type structure.[29] The c/a ratio in such structures serves as an indicator to predict whether the stacked 6^3 nets will distort ($c/a \approx 0.8$), with concomitant interlayer bond formation, or not ($c/a \approx 1.0$). For the stack of Ga_6 rings in $La_{13}Ga_8Sb_{21}$, this indicator (corresponding to the inter-ring spacing divided by the hexagon width) has a value of 1.056. The puckering in $La_{13}Ga_8Sb_{21}$ is therefore occurring for different reasons than in the family of structures with stacked 6^3 nets previously studied. To probe the origin of this puckering, we first examined a one-dimensional stack of planar Ga_6 rings (**7**) that are

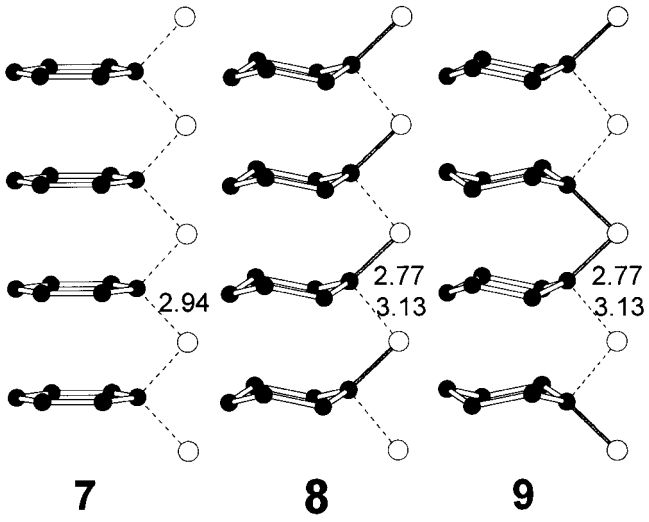

surrounded by the immediately neighboring Sb atoms, whose valence shells were artificially completed, to give $[Ga_6Sb_6]^{24-}$ (only one of the spokes of surrounding Sb atoms is shown in **7** for clarity). Although no evidence of long-range ordering of the puckered rings was detected in the crystal structure solution, two local orderings are possible: adjacent rings may be parallel (**8**), with all inter-ring Ga−Ga distances being 4.338(9) Å, or inverted (**9**), with three short 3.843(8) Å inter-ring Ga−Ga contacts. At the proposed electron count, our one-dimensional calculations reveal that either of the two limiting puckered stacking arrangements is more stable (−856.7 and −852.6 eV/f.u. for the parallel and inverted arrangements, respectively) than the undistorted planar arrangement (−841.9 eV/f.u.). The main consequence of the ring puckering is that Ga−Ga and Ga−Sb σ-type orbitals involving s−p hybrids on each Ga atom are mixed in with Ga−Ga π-type orbitals. This mixing tends to strengthen half of the Ga−Sb bonds (2.766(7) Å) surrounding a Ga_6 ring. For example, in the planar arrangement, the crystal orbital (at Γ) shown in **10** is Ga−Ga bonding but Ga−Sb antibonding; in the puckered arrangement, **11**, it becomes less Ga−Sb antibonding at the expense of slightly weakened Ga−

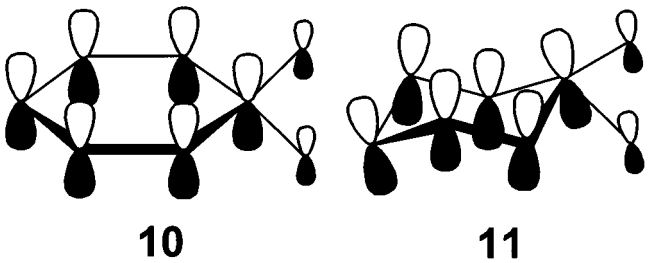

Ga bonding. There is little difference in energies between the parallel and inverted puckered arrangements, largely because the inter-ring Ga−Ga interaction is essentially nonbonding (MOP ~ 0). We consider only the (slightly) more stable parallel arrangement in our subsequent calculations.

We are now in a position to examine the entire $[Ga_6Sb_{15}]$ substructure. From the first retrotheoretical approach ($[Ga_6Sb_{15}] \leftarrow 3\,[Ga_2Sb_5]$), we proposed oxidation states of −1 for Ga, −2 for adjacent Sb, and −1 for inner

(29) Burdett, J. K.; Miller, G. J. *Chem. Mater.* **1990**, *2*, 12.

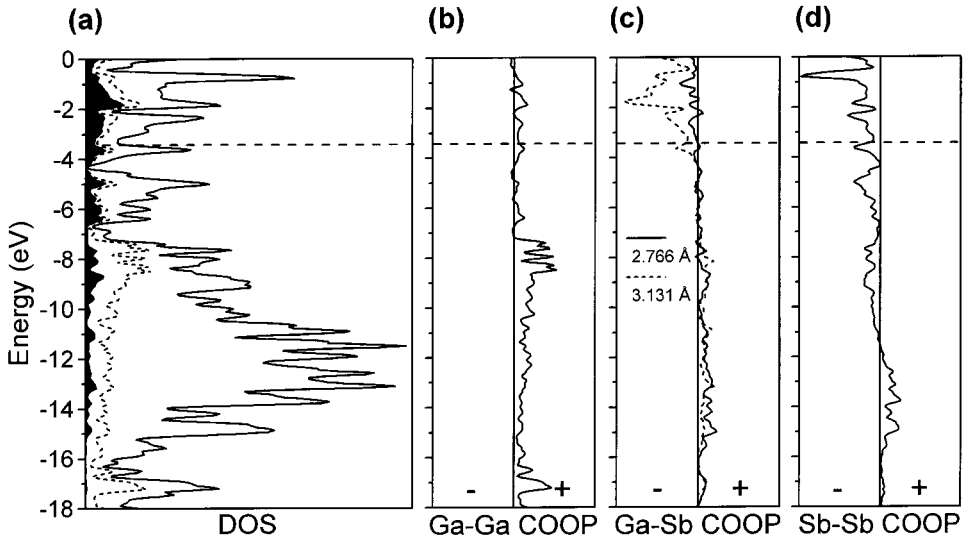

Figure 11. (a) Density of states (DOS) for the three-dimensional $[Ga_6Sb_{15}]^{27-}$ substructure of $La_{13}Ga_8Sb_{21}$. The Ga projection is shown by the short dashed line, and the filled area of this curve represents the Ga(p_z) projection; what remains of the DOS is the Sb projection. Crystal orbital overlap population (COOP) curves for the (b) Ga−Ga, (c) Ga−Sb, and (d) Sb−Sb interactions are also shown. The dashed horizontal lines in (a)−(d) represent the Fermi level at the proposed electron count.

Sb atoms, and we expected that Ga^{1-} atoms might have to be oxidized further, even after forming Ga−Ga bonds. From the second retrotheoretical approach ($[Ga_6Sb_{15}] \leftarrow [Ga_6] + 3[Sb_5]$), we saw that adjustments of Ga−Sb bonding interactions are necessary and that Sb−Sb bonds might have to weaken as well. The DOS curve for $[Ga_6Sb_{15}]^{27-}$ and the COOP curves for the Ga−Ga, Ga−Sb, and Sb−Sb interactions are shown in Figure 11. The $[Sb_5]$ ribbon interacts significantly with the Ga π block, which can be roughly gauged by the broad energy range in which the Ga(p_z) contribution makes to the DOS (Figure 11a) as well as the extensive mixing of Ga−Ga, Ga−Sb, and Sb−Sb character in the states as seen in the COOP curves (Figures 11b−d). As anticipated from Figure 10b, this increased dispersion results in a transfer of electrons from Ga to the Sb ribbon atoms, which is reflected in the Mulliken charges determined for the $[Ga_6Sb_{15}]^{27-}$ substructure (−0.56 for the Ga atoms, −1.62 for the adjacent Sb atoms, and −1.54 for the inner Sb atoms). The large overlap population of 0.89 calculated for the Ga−Ga bonds within the six-membered ring is consistent with strengthened Ga−Ga bonding expected as a result of the depopulation of π^* bands. The reduction of the ribbon Sb atoms causes a substantial proportion of Sb−Sb antibonding levels to be filled so that the overlap population becomes essentially zero (0.002) for the Sb−Sb interactions; the weakening of Sb−Sb bonding has proceeded a little too far, but as we shall see later, this can be remedied when the rest of the $La_{13}Ga_8Sb_{21}$ structure is also considered. The long and short Ga−Sb interactions between the Ga_6 rings and Sb ribbons have overlap populations of 0.33 and 0.60, respectively, which substantiate their description as a 3-center-2-electron bond with asymmetric distribution of electron density between the atoms.[8]

Assembling the Complete $La_{12}Ga_4Sb_{23}$ and $La_{13}Ga_8Sb_{21}$ Structures. At this stage, we are ready to re-assemble the composite $[Ga_4Sb_{23}]^{36-}$ and $[Ga_8Sb_{21}]^{39-}$ substructures of $La_{12}Ga_4Sb_{23}$ and $La_{13}Ga_8Sb_{21}$, respectively, from their component bonding networks. The overall charge (−36 or −39) is obtained

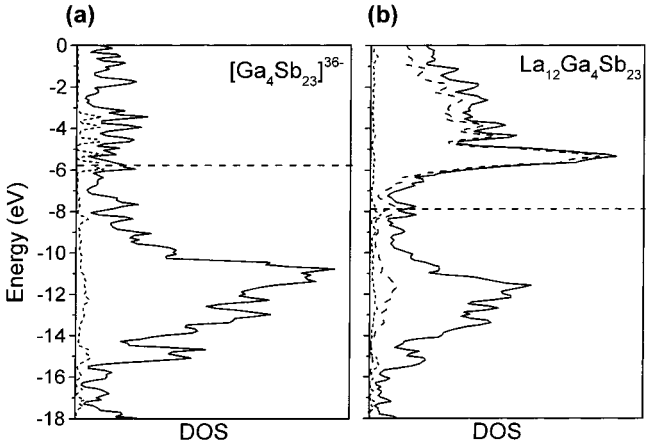

Figure 12. Density of states (DOS) for (a) the composite $[Ga_4Sb_{23}]^{36-}$ substructure and (b) the complete $La_{12}Ga_4Sb_{23}$ structure. The Ga projection is shown by the shorter dashed line, and the La projection in (b) is shown by the longer dashed line; what remains of the DOS is the Sb projection. The dashed horizontal lines in (a) and (b) indicate the Fermi levels.

assuming that the Zintl concept applies; that is, the La atoms transfer their valence electrons entirely. We can compare this electron count to that obtained by summing up the contributions of the individual components that were analyzed separately.

For $La_{12}Ga_4Sb_{23}$, the process is relatively straightforward. We assigned charges of −6, −7, and −16 to the noninteracting $[GaSb_3]$, $[Sb_5]$, and $[Ga_2Sb_{12}]$ networks, respectively. At these electron counts, the Fermi levels for the substructures lie at −10.5, −7.6, and −5.4 eV, respectively. The total charge for the $[Ga_4Sb_{23}]$ substructure obtained by combining these networks is −35: $[Ga_2Sb_{12}]^{16-}[Sb_5]^{7-}[GaSb_3]^{6-}[GaSb_3]^{6-}$. This count is one electron less than that required by the Zintl concept, suggesting that one of the networks must be further reduced. The DOS curve for the composite $[Ga_4Sb_{23}]^{36-}$ substructure is shown in Figure 12a. Because the Fermi level for $[Ga_4Sb_{23}]^{36-}$ is calculated to be at −5.8 eV, the $[GaSb_3]$ trigonal planes and $[Sb_5]$ ribbons are likely candidates for reduction. The one

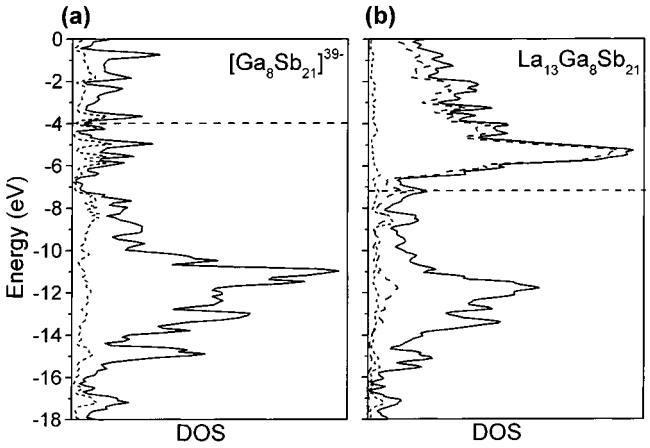

Figure 13. Density of states (DOS) for (a) the composite $[Ga_8Sb_{21}]^{39-}$ substructure and (b) the complete $La_{13}Ga_8Sb_{21}$ structure. The Ga projection is shown by the shorter dashed line, and the La projection in (b) is shown by the longer dashed line; what remains of the DOS is the Sb projection. The dashed horizontal lines in (a) and (b) indicate the Fermi levels.

extra electron per formula unit may be used for Ga−Ga bonding between $GaSb_3$ trigonal planes along a one-dimensional stack, just as they are in $La_{13}Ga_8Sb_{21}$. Although the crystal structure determination of $Pr_{12}Ga_4Sb_{23}$ shows that the $GaSb_3$ units are strictly planar, the elongation of the thermal ellipsoid along the c axis observed for the central Ga atom suggests that incipient interunit Ga−Ga bonds may be forming.[8] Alternatively, and perhaps more realistically, the $[Sb_5]$ ribbons may be reduced; the ability to act as an electron sink is often attributed to Sb square nets.[6b,9,18,30]

The re-assembly exercise for the composite $[Ga_8Sb_{21}]^{39-}$ substructure of $La_{13}Ga_8Sb_{21}$ is complicated by the disorder in the crystal structure.[8] At the −7 charge proposed for the one-dimensional $[GaSb_3]$ array, the most energetically favorable stacking arrangement (with a Fermi level of −6.2 eV) is that in which all adjacent $GaSb_3$ units are inverted with respect to one another. Our electronic structure calculations for the $[Ga_6Sb_{15}]$ network indicate that the stacking arrangement of the Ga_6 rings makes little difference to the total energy. For simplicity, we assume that all neighboring Ga_6 rings are parallel. At the −27 charge assigned to the $[Ga_6Sb_{15}]$ network, the Fermi level for this arrangement lies at −3.4 eV. In our hypothetical ordered model for the composite $[Ga_8Sb_{21}]$ substructure ($P\bar{3}$, $Z = 2$, $a = 17.657(2)$, $c = 8.676(2)$ Å), we double the c axis relative to the original crystal structure and reduce the symmetry from hexagonal to trigonal. The total charge for the $[Ga_8Sb_{21}]$ substructure obtained by combining these two networks is −41: $[Ga_6Sb_{15}]^{27-}[GaSb_3]^{7-}[GaSb_3]^{7-}$. This count is two electrons more than predicted by the Zintl analysis. The DOS curve for the ordered $[Ga_8Sb_{21}]^{39-}$ substructure is shown in Figure 13a, and the Fermi level is calculated to be at −4.0 eV. Because the Fermi level for the $[GaSb_3]$ array lies well below −4.0 eV, it is the $[Ga_6Sb_{15}]$ network that must be oxidized. The two electrons are removed from bands with Ga−Ga π bonding character and Sb−Sb antibonding character (Figures 11b,d). Accordingly, the oxidation of the $[Ga_6Sb_{15}]$ network results in slightly weakened Ga−Ga bonding (MOP of 0.87) and strengthened Sb−Sb bonding (MOP of 0.05).

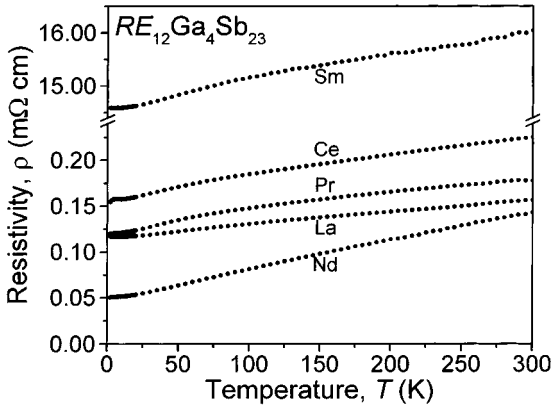

Figure 14. Temperature dependence of the resistivities of the $RE_{12}Ga_4Sb_{23}$ series.

Inclusion of the La atoms in the band structure calculations does not drastically alter the overall picture. The DOS curves for the complete $La_{12}Ga_4Sb_{23}$ and $La_{13}Ga_8Sb_{21}$ structures, with the La contributions also indicated, are shown in Figures 12b and 13b, respectively. Although we have initially considered the La atoms as isolated La^{3+} cations, a substantial number of La states are populated. The La d-block states overlap with Ga and Sb states, resulting in electron transfer from the metalloid atoms to La and an attendant lowering of the Fermi levels to −7.9 eV for $La_{12}Ga_4Sb_{23}$ or to −7.2 eV for $La_{13}Ga_8Sb_{21}$. The overlap populations calculated for the La−Ga and La−Sb interactions (0.06 and 0.21 for $La_{12}Ga_4Sb_{23}$; 0.09 and 0.20 for $La_{13}Ga_8Sb_{21}$, respectively) indicate significant covalency. Because the states that lie just below the Fermi levels in $[Ga_4Sb_{23}]^{36-}$ and $[Ga_8Sb_{21}]^{39-}$ are mainly Sb−Sb antibonding and Ga−Ga bonding in character, the reduction of the Fermi energies in the $La_{12}Ga_4Sb_{23}$ and $La_{13}Ga_8Sb_{21}$ band structures strengthens the Sb−Sb bonds of the channel-defining networks (MOP of 0.25 for $La_{12}Ga_4Sb_{23}$; MOP of 0.23 for $La_{13}Ga_8Sb_{21}$) and weakens the Ga−Ga bonds of the Ga_2 pairs (MOP of 0.72) or Ga_6 rings (MOP of 0.76), respectively. In each of the band structures, the Fermi level falls in a region of moderate DOS, crossing dispersive bands with contributions from La, Ga, and Sb. Metallic behavior is thus predicted for $La_{12}Ga_4Sb_{23}$ (and by analogy $RE_{12}Ga_4Sb_{23}$) and $La_{13}Ga_8Sb_{21}$.

Transport and Magnetic Measurements. Resistivity measurements confirm that all $RE_{12}Ga_4Sb_{23}$ members, in the 2−300 K temperature range (Figure 14), and $La_{13}Ga_8Sb_{21}$, in the 2.4−300 K range (Figure 15), are metallic. The resistivity data for $RE_{12}Ga_4Sb_{23}$ are summarized in Table 2. Most members of the series (RE = La−Nd) have resistivities on the order of 10^{-4} Ω cm, but $Sm_{12}Ga_4Sb_{23}$, with a resistivity on the order of 10^{-2} Ω cm, is a much poorer conductor. All members generally exhibit a monotonic decrease in resistivity with temperature. The sharp decrease in slope below ~5 K observed for $Ce_{12}Ga_4Sb_{23}$ may be a consequence of a loss in spin-disorder scattering at low temperatures. Similar behavior has been described for the antiferromagnetic Ce member of the $RE_6Ge_{5-x}Sb_{11+x}$ series of

(30) Ferguson, M. J.; Hushagen, R. W.; Mar, A. *J. Alloys Compd.* **1997**, *249*, 191.

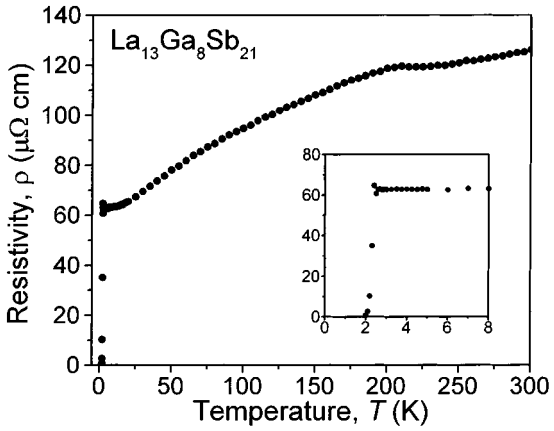

Figure 15. Temperature dependence of the resistivity of $La_{13}Ga_8Sb_{21}$. The inset gives an enlarged view showing the superconducting transition more clearly.

Table 2. Summary of Resistivity Data for $RE_{12}Ga_4Sb_{23}$

compound	ρ_{300K} (mΩ cm)	ρ_{300K}/ρ_{2K}
$La_{12}Ga_4Sb_{23}$	0.157	1.34
$Ce_{12}Ga_4Sb_{23}$	0.225	1.46
$Pr_{12}Ga_4Sb_{23}$	0.177	1.47
$Nd_{12}Ga_4Sb_{23}$	0.143	2.83
$Sm_{12}Ga_4Sb_{23}$	16.0	1.10

compounds.[31] We plan to make magnetic susceptibility measurements for $RE_{12}Ga_4Sb_{23}$ to investigate their magnetic properties at low temperatures. For RE = Ce, these studies will help determine if the drop in resistivity arises from the presence of long-range magnetic ordering.

The high-temperature transport behavior of $La_{13}Ga_8Sb_{21}$ ($\rho_{300K} = 1.26 \times 10^{-4}$ Ω cm, $\rho_{300K}/\rho_{2.4K} = 1.94$) resembles that observed for $La_{12}Ga_4Sb_{23}$, but at low temperatures, the resistivity drops abruptly to zero (Figure 15). This is assigned to a transition to a superconducting state with $T_c = 2.4$ K. Magnetic susceptibility measurements support this interpretation of the resistivity data: as shown in Figure 16, the onset of the characteristic diamagnetic response occurs below 2.5 K. However, the limiting diamagnetic susceptibility could not be reached because of instrumental constraints. The zero-field-cooled (ZFC) diamagnetic shielding and field-cooled Meissner effect curves measured with an applied field of 10 Oe are essentially superimposable in the temperature range examined. The temperature dependence of the ac magnetic susceptibility (χ'_{ac}) for three different applied field strengths under ZFC conditions is plotted in Figure 16. The superconducting transition broadens and shifts to slightly lower temperature with increasing field strength.

Conclusion

On the basis of our extended Hückel calculations (which are limited by their dependence on the availability of accurate atomic parameters), we are unable to provide a concrete explanation for the observation of

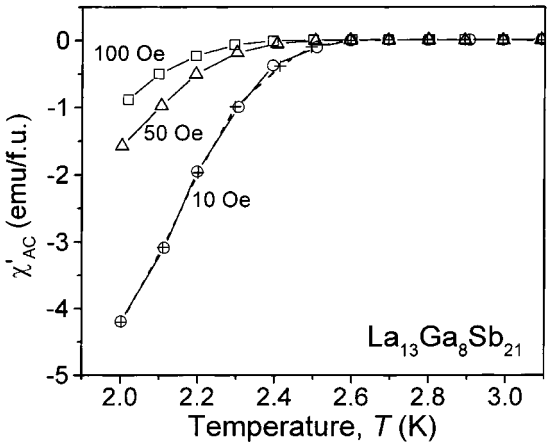

Figure 16. Temperature dependence of the zero-field-cooled ac magnetic susceptibility (χ'_{ac}) at three applied field strengths (○, 10; △, 50; □, 100 Oe) and of the field-cooled χ'_{ac} at 10 Oe (+) for $La_{13}Ga_8Sb_{21}$. The lines are included only to guide the eye.

superconductivity in $La_{13}Ga_8Sb_{21}$. However, we can speculate, in a very qualitative manner, on the origin of the superconductivity. The $La_{13}Ga_8Sb_{21}$ structure consists of classical covalently bonded $GaSb_3$ units enclosed in a nonclassical network, composed of $[Sb_5]$ ribbons connected by Ga_6 rings, containing delocalized bonding. In the band structure of $La_{13}Ga_8Sb_{21}$, narrow quasi-molecular bands, derived from the stacked $GaSb_3$ units, and dispersive bands originating from the channel-defining network are present near the Fermi level. In this respect, the electronic situation is similar to that in the superconducting carbide halides, such as $Y_2Br_2C_2$, in which an extensive rare-earth metal−metal bonding network, the source of band broadening, encloses discrete C_2 units that give rise to narrow bands.[10c] The coexistence of localized states and steep bands at the Fermi level has been proposed as a fingerprint in the search for superconductivity.[10] Although the crystal and electronic structures of $La_{12}Ga_4Sb_{23}$ are closely related to those of $La_{13}Ga_8Sb_{21}$, none of the $RE_{12}Ga_4Sb_{23}$ members undergoes a superconducting transition (down to 2 K). Because the precise location of the flat bands with respect to the Fermi level strongly influences superconductivity,[32] the difference in the physical properties of $La_{12}Ga_4Sb_{23}$ ($\varepsilon_f = -7.9$ eV) and $La_{13}Ga_8Sb_{21}$ ($\varepsilon_f = -7.2$ eV) is not surprising. Nevertheless, the appearance of superconductivity in $La_{13}Ga_8Sb_{21}$, a compound at the "Zintl border" featuring classical and nonclassical bonding networks, provides impetus for the continued exploration of systems with reduced electronegativity differences between the component atoms.

Acknowledgment. This work was supported by the Natural Sciences and Engineering Research Council of Canada and the University of Alberta. We thank Christina Barker for assistance with the EDX analyses.

CM0014132

(31) Deakin, L.; Lam, R.; Mar, A. *Inorg. Chem.* **2001**, *40*, 960.

(32) Kleinke, H.; Waldeck, M.; Gütlich, P. *Chem. Mater.* **2000**, *12*, 2219.